DOI: 10.1002/ejic.200601184

Phosphane and Phosphite Unsymmetrically Disubstituted Diiron Complexes Related to the Fe-Only Hydrogenase Active Site

Ping Li,[a] Mei Wang,*[a] Chengjiang He,[a] Xiaoyang Liu,[a,b] Kun Jin,[a] and Licheng Sun*[a,c]

Keywords: Bioinorganic chemistry / Carbonyl displacement / Diiron complexes / Fe-only hydrogenase / P ligands

A series of unsymmetrically disubstituted diiron complexes [(μ-pdt){$Fe(CO)_2L^1$}{$Fe(CO)_2L^2$}] [pdt = 1,3-propanedithiolato; $L^1 = PMe_3$, $L^2 = PMe_2Ph$, **4**; PPh_3, **5**; PCy_3, **6**; $P(OEt)_3$, **7**; $L^1 = PMe_2Ph$, $L^2 = PPh_3$, **8**; $P(OEt)_3$, **9**; $L^1 = P(OEt)_3$, $L^2 = PPh_3$, **10**; PCy_3, **11**] and [(μ-edt){$Fe(CO)_2PMe_3$}{$Fe(CO)_2PPh_3$}] (edt = 1,2-ethanedithiolato, **12**) were prepared by means of stepwise CO displacements of [(μ-pdt)$Fe_2(CO)_6$] and [(μ-edt)-$Fe_2(CO)_6$] by different tertiary phosphane and phosphite ligands. The interconversion of the irondithiacyclohexane ring and the rotation of the [$Fe(CO)_2PR_3$] subunit were studied using by variable-temperature $^{31}P\{^1H\}$ NMR spectroscopy of **4**, **6** and **12** in solution. The molecular structures of **4**–**6**, **8**–**10** and **12** show that complexes **4**–**6**, **8**, **9** and **12** possess an apical/basal coordination mode and complex **10** has an apical/apical conformation. The X-ray analyses indicate that the PMe_2Ph ligand in the apical position of the starting complex [(μ-pdt){$Fe(CO)_3$}{$FeCO_2(PMe_2Ph)$}] rotates to the basal position on conversion to the products **8** and **9**. Cyclic voltammograms of **4**–**11** were studied both under argon and CO. The influences of the phosphane and phosphite ligands on the redox properties of the unsymmetrically disubstituted diiron complexes are discussed.

Introduction

Iron-only hydrogenases with popular metals and simple diatom ligands in their active sites can catalyse the proton reduction to molecular hydrogen more efficiently than other types of hydrogenases. In recent years, synthesis of structural and functional models of the Fe-only hydrogenase active site has been a hot topic in bioinorganic and organometallic chemistry. The well-studied organometallic diiron complex [(μ-pdt)$Fe_2(CO)_6$] (pdt = 1,3-propanedithiolato) serves as a synthetic model of the Fe-only hydrogenase active site in terms of the structure revealed by X-ray crystallographic studies.[1,2] Various good donor ligands, such as CN^-,[3–9] PR_3,[8–17] CNR[18,19] and NHC (N-heterocyclic carbene)[20,21] have been successfully introduced to the model complexes by CO displacement in order to investigate the electrochemistry and protonation properties of the derivatives. Tertiary phosphane ligands, which can avoid the intricacy of the protonation process on the cyanide nitrogen atom, are widely used in many model complexes of the Fe-only hydrogenase, especially for hydridodiiron dithiolate complexes.[22–24] Although the CO displacement of [(μ-$SR)_2$-$Fe_2(CO)_6$] (R = Me, Et, Ph), [(μ-edt)$Fe_2(CO)_6$] (edt = 1,2-ethanedithiolato), [(μ-pdt)$Fe_2(CO)_6$] and [(μ-adt)$Fe_2(CO)_6$] (adt = 2-azapropane-1,3-dithiolato) by tertiary phosphanes has been extensively studied,[10–17] to the best of our knowledge the model complexes in the form of [(μ-pdt){$Fe(CO)_2$-L^1}{$Fe(CO)_2L^2$}] with two different π ligands have been scarcely reported.[10] To continue a systematic study of the influence of phosphane and phosphite ligands on the coordination structures, the reactivity and the redox properties of the iron centres,[15] a series of unsymmetrically disubstituted model complexes [(μ-pdt){$Fe(CO)_2L^1$}{$Fe(CO)_2L^2$}] [$L^1 = PMe_3$, $L^2 = PMe_2Ph$, **4**; PPh_3, **5**; PCy_3, **6**; $P(OEt)_3$, **7**; $L^1 = PMe_2Ph$, $L^2 = PPh_3$, **8**; $P(OEt)_3$, **9**; $L^1 = P(OEt)_3$, $L^2 = PPh_3$, **10**; PCy_3, **11**] and [(μ-edt){$Fe(CO)_2PMe_3$}{$Fe(CO)_2$-PPh_3}] (**12**) with two different tertiary phosphane and phosphite ligands were prepared and among them **4**–**6**, **8**–**10** and **12** were crystallographically characterised. Here we describe the preparation, variable-temperature $^{31}P\{^1H\}$ NMR spectra, molecular structures and cyclic voltammograms of diiron complexes unsymmetrically disubstituted by phosphane and phosphite ligands.

[a] State Key Laboratory of Fine Chemicals, DUT-KTH Joint Education and Research Centre on Molecular Devices, Dalian University of Technology (DUT),
Zhongshan Road 158-46, Dalian 116012, China
E-mail: symbueno@dlut.edu.cn
[b] State Key Laboratory of Inorganic Synthesis and Preparative Chemistry, Jilin University,
Changchun 130012, China
[c] Department of Chemistry, Royal Institute of Technology (KTH),
10044 Stockholm, Sweden
Supporting information for this article is available on the WWW under http://www.eurjic.org or from the author.

Results and Discussion

Preparation and Spectroscopic Characterisation of Complexes 4–12

The monosubstituted complexes $[(\mu\text{-pdt})Fe_2(CO)_5L^1]$ [L^1 = PMe_3, **1**; PMe_2Ph, **2**; $P(OEt)_3$, **3**] were prepared in moderate yields according to the previous report.[15] Treatment of **1** with PMe_2Ph, PPh_3 and $P(OEt)_3$ in toluene at reflux afforded products **4**, **5** and **7**, respectively, in good yields (Scheme 1). Complex **6** could be obtained from **1**, in a moderate yield, in the presence of 1 equiv. of PCy_3 using Me_3NO as a CO-removing reagent. The disubstituted complexes **4**, **8** and **9** were obtained in yields of 40–70% by the replacement of CO in **2** with 1 equiv. of the corresponding tertiary phosphane or phosphite ligand in toluene at reflux (Scheme 2). Complexes **7** and **9** could also be prepared by treatment of **3** with a slight excess of PMe_3 and PMe_2Ph under the same conditions (Scheme 3). The reaction of complex **3** with 1 equiv. or an excess of PPh_3 in toluene at reflux did not afford complex **10**, presumably due to the high activation energy caused by the large bulk and weak donating capability of the PPh_3 ligand. Consequently, Me_3NO was used as CO removing reagent to prepare complex **10** (Scheme 3). Although the volume of PCy_3 is larger than that of PPh_3, complex **11** could be obtained in a good yield from a solution of **3** and 1 equiv. of PCy_3 in toluene at reflux. The stronger donating capability of PCy_3 benefits the PCy_3/CO displacement. Complex **12** was prepared according to a similar procedure used for **5**. The unsymmetrically disubstituted diiron dithiolate complexes **4**–**12** are relatively thermally and air-stable in the solid state.

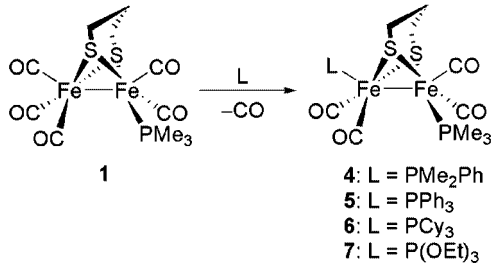

Scheme 1.

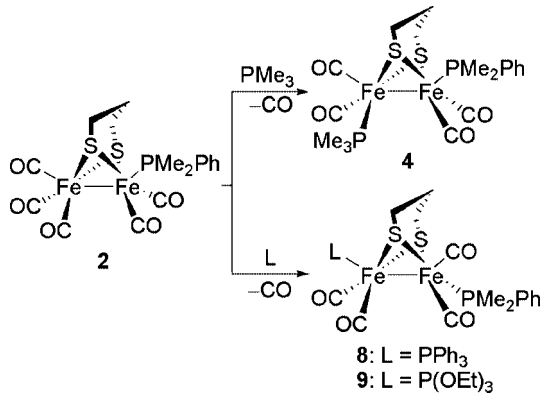

Scheme 2.

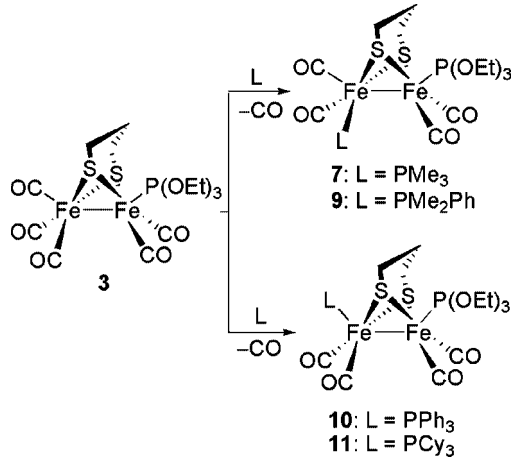

Scheme 3.

The products **4**–**12** were characterised by ESI- or APCI-MS, IR, ^1H and $^{31}P\{^1H\}$ NMR spectroscopy as well as elemental analysis. The results of the elemental analyses for all products are in good agreement with the proposed compositions. The $[M + H]^+$ peaks of all the diiron dithiolates were detected in the mass spectra in ESI- or APCI-positive mode. The disubstituted complexes **4**–**11** each display three ν(CO) bands in the region of 1900–2000 cm^{-1}. The IR data of ν(CO) for **4**–**11** are listed in Table 1 together with the

Table 1. A comparison of ν(CO) bands of **1**–**11** and the all-CO parent complex in CH_3CN.

Complex	L^1, L^2	ν(CO)/cm^{-1}	$\Delta\nu(CO)_{av}$/cm^{-1}[a]
All-CO complex	–	2074 (m), 2036 (s), 1995 (s)	–
1	PMe_3, –	2037 (s), 1980 (s), 1919 (m)	56
2	PMe_2Ph, –	2040 (s), 1980 (s), 1921 (m)	55
3	$P(OEt)_3$, –	2046 (s), 1989 (s), 1936 (m)	45
4	PMe_3, PMe_2Ph	1981 (m), 1943 (s), 1908 (m)	91
5	PMe_3, PPh_3	1985 (s), 1946 (s), 1905 (s)	90
6	PMe_3, PCy_3	1976 (s), 1937 (s), 1901 (s)	97
7	PMe_3, $P(OEt)_3$	1991 (s), 1949 (s), 1907 (s)	86
8	PMe_2Ph, PPh_3	1982 (s), 1946 (s), 1913 (s)	88
9	PMe_2Ph, $P(OEt)_3$	1991 (s), 1952 (s), 1922 (s)	80
10	$P(OEt)_3$, PPh_3	1997 (s), 1955 (s), 1934 (s)	73
11	$P(OEt)_3$, PCy_3	1993 (s), 1943 (s), 1933 (s)	79

[a] $\Delta\nu(CO)_{av} = [\Sigma\nu(CO)_{all\text{-}CO} - \Sigma\nu(CO)]/3$.

ν(CO) data of complexes **1**–**3** and the all-CO complex.[15,25] A comparison of the ν(CO) bands for the three subsets (**1** vs. **4**–**7**, **2** vs. **4**, **8** and **9**, and **3** vs. **7** and **9**–**11**) of complexes **4**–**11** shows that the introduction of the second phosphane and phosphite ligand has a considerable effect on the ν(CO) bands of the diiron complexes. The variation of the ν(CO) bands implies the influence of different tertiary phosphane and phosphite ligands on the electron density of the Fe centres. Compared with the all-carbonyl complex, the average values of the three strong ν(CO) bands are red-shifted by 73–97 cm^{-1} for **4**–**11**. The shift values [$\Delta\nu(CO)_{av}$] are consistent with the electron-donating capabilities of different phosphane and phosphite ligands.

Variable-Temperature $^{31}P\{^1H\}$ NMR Spectra of Complexes 4, 6 and 12

The variable-temperature $^{31}P\{^1H\}$ NMR spectra of **4**, **6** and the edt-bridged analogue **12** are shown in Figures 1 and 2. Complexes **4** and **6** each display two signals at δ = 25.5 and 29.6 ppm for **4**, and δ = 23.3 and 68.1 ppm for **6**, in the $^{31}P\{^1H\}$ NMR spectra at room temperature [Figure 1(a) and (b)]. On lowering the temperature, each $^{31}P\{^1H\}$ NMR signal of complex **4** splits into two resonances (δ = 26.5, 26.8 for PMe_3 and δ = 32.5, 33.3 ppm for PMe_2Ph) at –80 °C [Figure 1(a′) and the inset]. Two resonances for the PMe_3 ligand and two broad signals for the PCy_3 ligand can be observed for complex **6** at –80 °C [Figure 1(b′)]. The broad resonance of the PCy_3 ligand may result from the slow rotation of the bulky PCy_3 ligand. The splitting of the $^{31}P\{^1H\}$ NMR signals at low temperature can be attributed to the slowing down of the interconversion of the FeS_2C_3 six-membered rings in complexes **4** and **6**. The resonance difference for the PMe_3 ligand of **6** (δ = 2.4 ppm) is apparently larger than that for the splitting of the PMe_3 ligand of **4** (δ = 0.3 ppm), presumably due to the large interaction between the propanedithiolato group and the bulky PCy_3 ligands. A similar interconversion of the irondithiacyclohexane rings in the symmetrically PR_3-disubstituted diiron complexes has been previously reported by Darensbourg and co-workers.[13,26]

To explore the rotation flexibility of phosphane ligands of the $[Fe(CO)_2PR_3]$ subunit and to avoid the interconversion of the S-to-S bridge, an edt-bridged analogue [(μ-edt){$Fe(CO)_2PMe_3$}{$Fe(CO)_2PPh_3$}] (**12**) was prepared for study by variable-temperature $^{31}P\{^1H\}$ NMR spectroscopy. Complex **12** displays two ^{31}P resonances at δ = 22.7 ppm for PMe_3 and δ = 60.3 ppm for PPh_3 at room temperature [Figure 2(top)]. When the measuring temperature was lowered to –80 °C, four ^{31}P signals were observed for the edt-bridged diiron complex **12** [Figure 2(bottom)], two strong signals at δ = 27.3 ppm for PMe_3, δ = 60.7 ppm for PPh_3 and two weak signals at δ = 17.0 ppm for PMe_3 and δ = 59.9 ppm for PPh_3. It is noticeable that the large resonance difference (10.3 ppm) between the two ^{31}P signals for the PMe_3 ligand of **12** can be observed, while the difference for the PPh_3 ligand is only 0.8 ppm. A rational explanation for the obtained variable-temperature $^{31}P\{^1H\}$ NMR spectra of **12** is that the splitting of the ^{31}P resonances at low temperature is caused by the slowing down of the rotation of the subunit $[Fe(CO)_2PMe_3]$,[13] and the subunit $[Fe(CO)_2PPh_3]$ does not rotate in solution within the range between –80 and 25 °C but maintains its apical position as in the crystalline state. Accordingly, the two strong signals can be attributed to the major apical (PPh_3)/basal (PMe_3) isomer of **12** and the two weak signals to the ap/ap isomer. The $^{31}P\{^1H\}$ NMR spectra of **12** suggest that the coordination

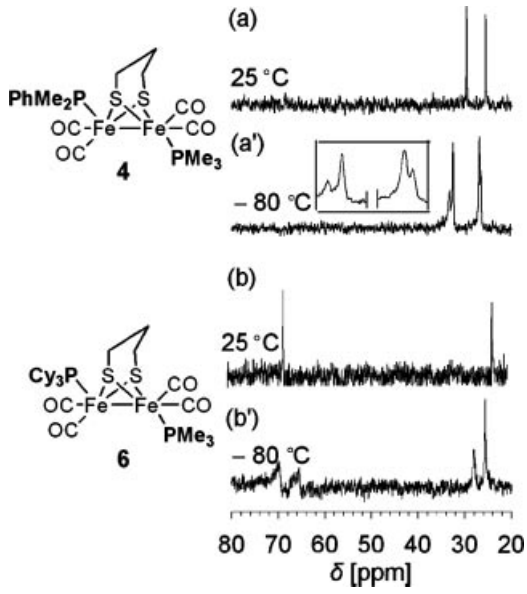

Figure 1. Variable-temperature $^{31}P\{^1H\}$ NMR spectra of **4** and **6** in $CDCl_3$.

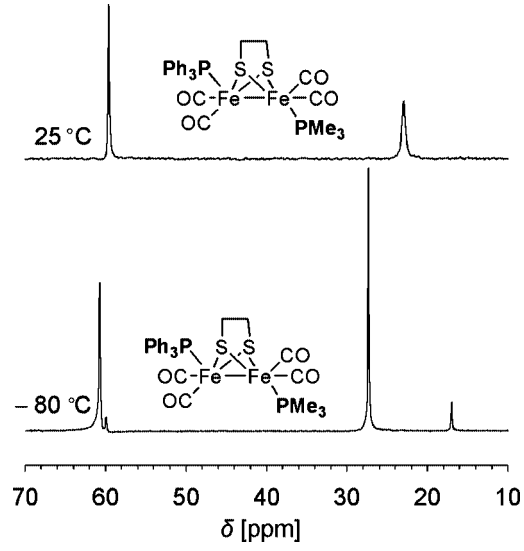

Figure 2. $^{31}P\{^1H\}$ NMR spectra of **12** at variable temperature in $CDCl_3$.

orientation of the PMe_3 ligand in the $[Fe(CO)_2PMe_3]$ subunit does not exhibit an apparent effect on the chemical shift of the PPh_3 ligand attached to the vicinal iron atom.

Molecular Structures of Complexes 4–6, 8–10 and 12

Single-crystal X-ray diffraction studies were carried out on complexes **4**–**6**, **8**–**10** and **12** to determine the coordination conformations of the phosphane and phosphite ligands in the diiron complexes. The molecular structures of **4**–**6**, **8**–**10** and **12** are presented in Figure 3 and selected bond lengths and angles are listed in Table 2. The central 2Fe2S cores of complexes **4**–**6**, **8**–**10** and **12** are all in butterfly conformation as for previously reported model complexes[10–15] and each iron atom is coordinated with a distorted square-pyramidal geometry. The vertex carbon atoms of the FeS_2C_3 six-membered rings all orient to the phenyl-containing phosphane ligands, either in apical (**4**, **5** and **10**) or in basal (**9**) positions. In contrast, the ellipsoid of the vertex carbon atom C(14) is disordered in the crystalline state of **8** with two phenyl-containing phosphane ligands attached to two iron atoms. The distances of the Fe–Fe bonds in **4**–**6**, **8** and **9** are quite similar (2.534–2.544 Å), while the Fe–Fe bond of **10** [2.5077(5) Å] with an ap/ap conformation is apparently shorter than that of its analogous ap/ba isomers **4**–**6**, **8** and **9**. The Fe–Fe bond [2.5553(4) Å] of the edt-bridged diiron complex **12** is longer than those of the pdt-bridged complexes. The dihedral angle, defined by the S(1)Fe(1)Fe(2) and S(2)Fe(1)Fe(2) planes, increases to 73.30(2)° for **10** featuring two bulky ligands as compared to 70.89(3)° for **4** bearing two small ligands and it increases to 77.72(2)° when the pdt-bridge is replaced by the edt-bridge. The dihedral angle is affected by the steric interactions between the phosphane or phosphite ligand and the S-to-S linker.

The X-ray diffraction analyses clearly show that the conformations of the two coordinating phosphane and phosphite ligands in complexes **4**–**6**, **8**, **9** and **12** are predominantly determined by the relative sizes of the ligands. Complexes **4**–**6**, **8**, **9** and **12** feature an ap/ba conformation in the crystalline state which is a common conformation for double-CO displacement by two non-carbonyl ligands on each iron atom of $[(\mu\text{-pdt})Fe_2(CO)_6]$.[4,9,20] The size of the second phosphane or phosphite ligand determines the orientation of the PMe_2Ph group in complexes **4**, **8** and **9**, which is in the apical position of **4** with PMe_3 as its counterpart and in the basal positions of **8** and **9** with PPh_3 or $P(OEt)_3$ on the other iron atom. Complex **10** containing two bulky ligands possesses an ap/ap conformation which, to the best of our knowledge, is the first structurally characterised unsymmetrically disubstituted diiron dithiolate complex of the ap/ap conformation except for the symmetrically PMe_2Ph-, $PPh_2(BrC_6H_4)$- and CN-*t*-Bu-disubstituted analogues.[15,19,27] Our previous crystallographic studies clarified that the ligand PMe_2Ph in the starting complex **2** is in an apical orientation.[15] The basal position of the PMe_2Ph ligand in **8** and **9** clearly verifies the conformational mobility of the $[Fe(CO)_2PMe_2Ph]$ subunit of the diiron dithiolate model complex in solution.

Cyclic Voltammograms of Complexes 4–11

The cyclic voltammograms (CVs) of complexes **4**–**11** were studied to evaluate the effects of different phosphane ligands on the redox properties of the iron atoms. Except for **6** and **11**, the CV measurements were carried out in CH_3CN for all complexes. The CVs of complexes **6** and **11** were recorded in toluene/CH_3CN (1:3, v/v) because of the poor solubility of **6** and **11** in CH_3CN.

Under argon, complexes **5**, **8** and **10** containing a PPh_3 ligand each display two reduction peaks in the range of –1.98 to –2.26 V (vs Ag/Ag^+, 0.01 M $AgNO_3$) in their CVs

Table 2. Selected bond lengths [Å] and angles [°] for **4**–**6**, **8**–**10** and **12**.

Complex	**4**	**5**	**6**	**8**	**9**	**10**	**12**
Bond lengths							
Fe–Fe	2.5430(5)	2.5383(6)	2.5375(5)	2.5437(10)	2.5341(9)	2.5077(5)	2.5553(4)
Fe–S[a]	2.2643(8)	2.2636(7)	2.2741(7)	2.2658(11)	2.2625(14)	2.2745(7)	2.2494(6)
$Fe–P_{ap}$	2.2299(7)	2.2518(7)	2.2822(7)	2.2534(10)	2.1589(13)	2.2117(7)[b]	2.2444(5)
$Fe–P_{ba}$	2.2335(6)	2.2312(8)	2.2293(8)	2.2352(11)	2.2278(13)	–	2.2198(6)
$Fe–C_{ap}$	1.755(2)	1.767(2)	1.762(3)	1.762(4)	1.768(5)	–	1.764(2)
$Fe–C_{ba}$[c]	1.777(2)	1.756(2)	1.758(3)	1.768(4)	1.764(4)	1.771(2)[d]	1.759(2)
S···S	3.053	3.039	3.039	3.044	3.039	3.045	2.877
Bond angles							
S–Fe–S[e]	84.77(2)	84.35(2)	83.86(3)	84.41(4)	84.38(5)	84.04(2)	79.65(2)
Fe–S–Fe[f]	68.33(2)	68.20(2)	67.82(2)	68.30(4)	68.12(4)	66.91(2)	69.34(2)
Dihedral[g]	70.89(3)	71.65(2)	72.75(2)	71.47(4)	71.68(5)	73.30(2)	77.72(2)

[a] Average over four Fe–S bonds. [b] Average over two $Fe–P_{ap}$ bonds. [c] Average over three $Fe–C_{ba}$ bonds. [d] Average over four $Fe–C_{ba}$ bonds. [e] Average over two S–Fe–S angles. [f] Average over two Fe–S–Fe angles. [g] Defined by the intersection of the two SFe_2 planes.

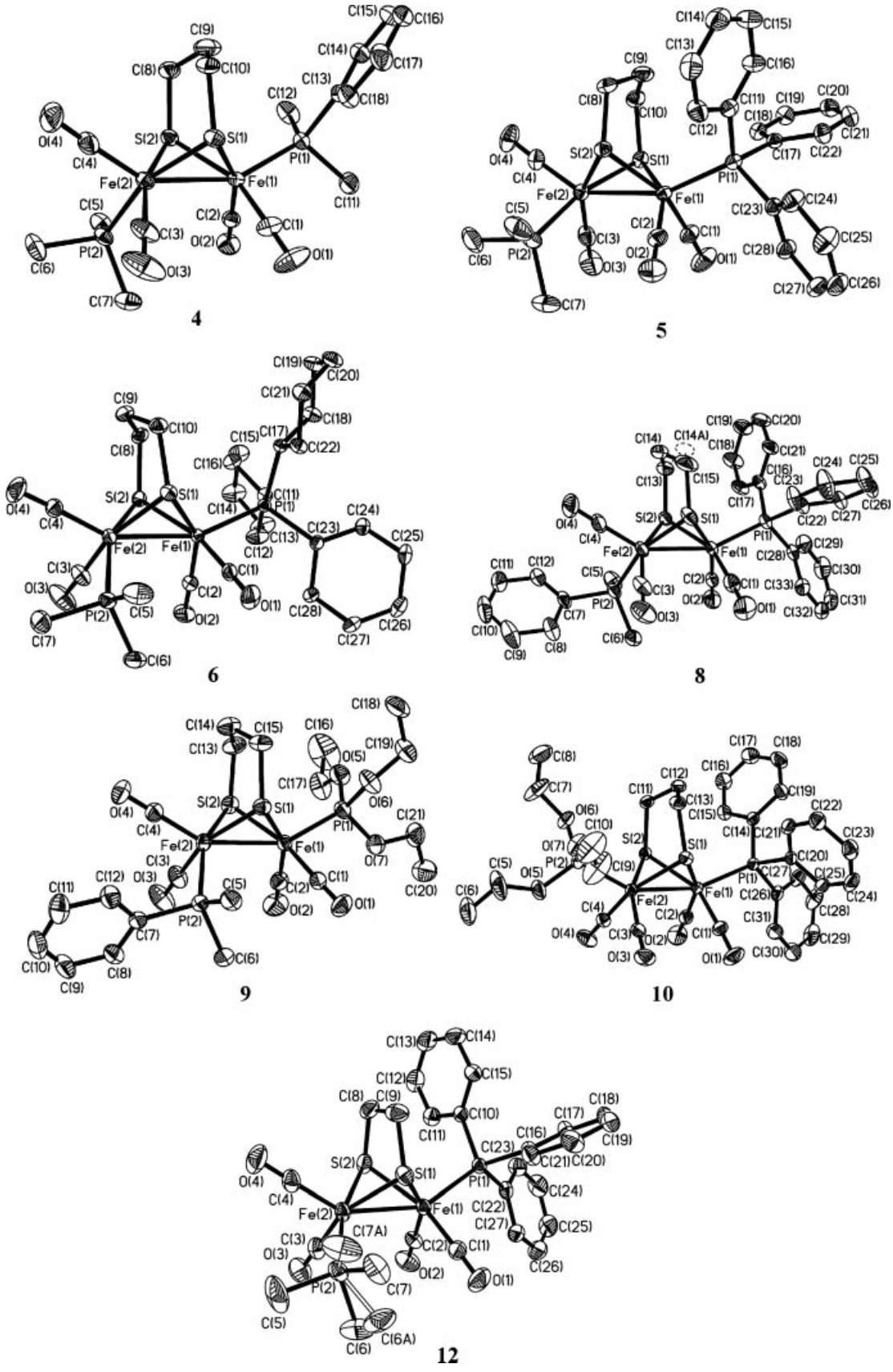

Figure 3. Molecular structures of **4**, **5**, **6**, **8**, **9**, **10** and **12** with thermal ellipsoids drawn at the 30% probability level. Hydrogen atoms have been omitted for clarity.

[Figure 4(a) for **5**] and the other complexes **4**, **6**, **7**, **9** and **11** without PPh_3 ligands each show a broad peak including two overlapping reduction events from –2.09 to –2.28 V [Figure 4(b) for **9**]. Considering the small potential differences of the two reduction peaks for each complex, the second reduction peak cannot be attributed to the further reduction process of Fe^IFe^0 to Fe^0Fe^0. In order to assign the reduction peaks, CVs of **4**–**11** were performed under CO in a CO-saturated CH_3CN solution. As the two sub-groups display similar CVs under CO (complexes with a PPh_3 ligand and those without PPh_3 ligand), we chose complexes **5** and **9** as examples for comparison of the CVs recorded under argon and under CO (Figure 4). The CVs of other complexes (**4**, **6**–**8**, **10** and **11**) under argon and under CO are given in the Supporting Information.

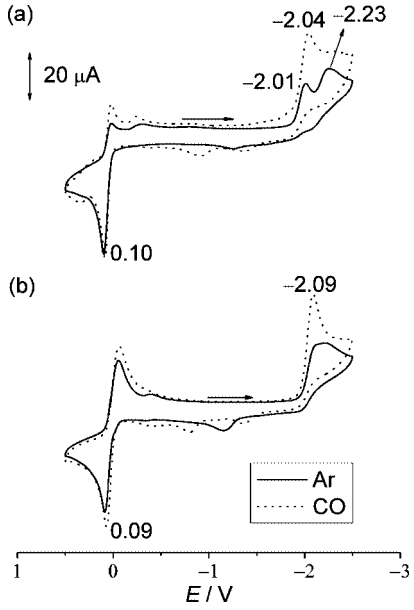

Figure 4. Cyclic voltammograms of complexes **5** (a) and **9** (b) under argon and under CO; 1.0 mM diiron complex, 0.05 M nBu_4NPF_6 in CH_3CN, scan rate 0.1 V s^{-1}.

The current of the first reduction peak at –2.01 V in the CV of **5**, which has been assigned to the Fe^IFe^I/Fe^IFe^0 process, increases under CO relative to that detected under argon. In the meantime the current height of the second reduction peak at –2.23 V apparently decreases when compared with that detected under argon. Similarly, the broad reduction peak in the range of –2.0 to –2.5 V for complex **9** under argon changes to a sharp reduction peak at –2.09 V under CO and the more cathodic overlapping peak disappears. The peak at –2.09 V can be attributed to the Fe^IFe^I/Fe^IFe^0 process. The different CVs recorded under argon and under CO reminded us of similar changes in the CVs reported for PMe_2Ph- and pta- (1,3,5-triaza-7-phosphaadamantane) -monosubstituted complexes[14,15] in which the second peaks detected under argon or N_2 may be attributed to a solvent-substituted species resulting from the 19-electron radical anion formed at the first reduction process. Furthermore, it was found that the current height ratio [*i*(I)/*i*(II)] of the two reduction peaks under argon varies with the scan rate. The *i*(I)/*i*(II) ratio increases when the CV is recorded at a higher scan rate. As shown in Figure 5, the values of the *i*(I)/*i*(II) ratios are ca. 1.0, 2.0 and 3.3 at scan rates of 0.1, 0.4 and 1.0 V s^{-1}, respectively. The CVs of multiple scans for complex **5** at a scan rate of 4.0 V s^{-1} show that the current height of the second reduction peak apparently increases in the second scan cycle accompanied by a decrease in the height of the first reduction peak (see Supporting Information). After three scan cycles, the current height ratio of the two reduction peaks does not exhibit any observable change. In view of the results of the CO control experiments, the variable scan rate measurements and the CVs of multiple scans, the second reduction peak detected under argon, either as a separated peak for the complex with a PPh_3 ligand or as an overlapping peak for the complex without PPh_3, is most likely due to the reduction of a new complex, presumably generated by a quick chemical reaction following the first reduction of the diiron(I,I) complex. In comparison, the reported symmetrically disubstituted diiron analogues $[(\mu\text{-pdt})\{Fe(CO)_2L\}_2]$ [L = PMe_3, PMe_2Ph, $P(OEt)_3$, pta] each exhibit only one reduction peak in the Fe^IFe^I/Fe^IFe^0 region of the CVs.[14,15,27] It seems that the reductive $[Fe^IFe^0]$ intermediates formed by the unsymmetrically disubstituted diiron complexes, especially the complexes containing a PPh_3 ligand, are less stable than those derived from the symmetrically disubstituted diiron analogues.

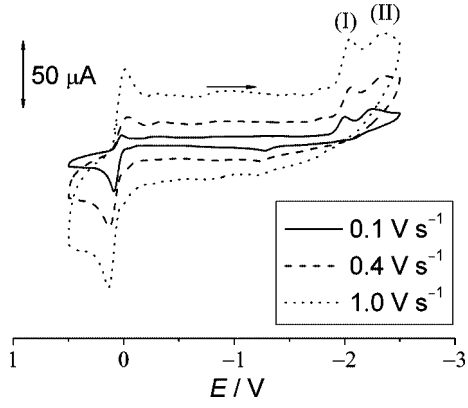

Figure 5. Cyclic voltammograms of complex **5** (1.0 mM) under argon; scan rate 0.1 [*i*(I)/*i*(II) = 1.0], 0.4 [*i*(I)/*i*(II) = 2.0] and 1.0 V s^{-1} [*i*(I)/*i*(II) = 3.3].

The redox potentials under CO for complexes **4**–**11** are listed in Table 3. The anodic peaks at –0.02 to +0.21 V have been assigned to the first oxidation process of Fe^IFe^I to $Fe^{II}Fe^I$ as described in the literature.[28] Complexes **6**, **7** and **9**–**11** exhibit quasi-reversible oxidation peaks, while **4**, **5** and **8** display irreversible peaks for the first oxidation process. It is interesting to notice that the $P(OEt)_3$ and PCy_3 ligands show a certain capability to stabilise the $Fe^{II}Fe^I$ species formed in the first oxidation process. This phenomenon was also observed in the CVs of the previously prepared

$P(OEt)_3$ and PMe_2Ph symmetrically disubstituted complexes.[15] The Fe^IFe^I to $Fe^{II}Fe^I$ oxidative peak was quasi-reversible for $[(\mu\text{-pdt})\{Fe(CO)_2P(OEt)_3\}_2]$ and totally irreversible for $[(\mu\text{-pdt})\{Fe(CO)_2PMe_2Ph\}_2]$. The redox potentials of **4**–**11** are consistent with the electron-donating capabilities of the phosphane and phosphite ligands. Complex **6** containing PMe_3 and PCy_3 displays the most negative redox potentials, –0.02 V for the oxidation process of Fe^IFe^I to $Fe^{II}Fe^I$ and –2.15 V for the Fe^IFe^I to Fe^IFe^0 process. In contrast, complex **10** featuring $P(OEt)_3$ and PPh_3 shows the most positive redox potentials, +0.21 V for the oxidation process of Fe^IFe^I to $Fe^{II}Fe^I$ and –1.98 V for the Fe^IFe^I to Fe^IFe^0 process. In general, the variations in the redox potentials by changing phosphane and phosphite ligands are ca. 230 mV for the first oxidation process and ca. 170 mV for the first reduction process.

Table 3. Redox potentials of complexes **4**–**11**.[a]

Complex	L^1, L^2	E_{pa}/V $Fe^IFe^I/Fe^{II}Fe^I$	E_{pc}/V Fe^IFe^I/Fe^IFe^0
4	PMe_3, PMe_2Ph	0.0	–2.12
5	PMe_3, PPh_3	+0.10	–2.04
6[b]	PMe_3, PCy_3	–0.02	–2.15
7	PMe_3, $P(OEt)_3$	+0.11	–2.08
8	PMe_2Ph, PPh_3	+0.11	–2.01
9	PMe_2Ph, $P(OEt)_3$	+0.09	–2.09
10	$P(OEt)_3$, PPh_3	+0.21	–1.98
11[b]	$P(OEt)_3$, PCy_3	+0.14	–2.14

[a] nBu_4NPF_6 (0.05 M) in a CO-saturated CH_3CN solution under CO; scan rate: 0.1 $V s^{-1}$; working electrode: glassy carbon electrode of diameter 3 mm; reference electrode: non-aqueous Ag/Ag^+ electrode (0.01 M $AgNO_3$ in CH_3CN); counter electrode: platinum wire. [b] Data collected in CO-saturated toluene/CH_3CN (1:3, v/v) mixture.

Conclusions

Nine unsymmetrically disubstituted diiron dithiolate complexes **4**–**12** with various phosphane and phosphite ligands were prepared and well characterised. The rotation of the $[Fe(CO)_2PMe_3]$ subunit can be detected by the variable-temperature $^{31}P\{^1H\}$ NMR spectra of **12**, which also suggest that the $[Fe(CO)_2PPh_3]$ subunit does not rotate in solution in the range between –80 and 25 °C. In the substitution reactions of $[(\mu\text{-pdt})\{Fe(CO)_3\}\{Fe(CO)_2PMe_2Ph\}]$ (**2**) by PPh_3 and $P(OEt)_3$, the PMe_2Ph ligand in the apical position of **2** moves to the basal position on formation of the products **8** and **9** and this provides clear evidence for the conformational flexibility of the $[Fe(CO)_2PMe_2Ph]$ subunit in solution. The CVs of complexes **4**–**11** under argon and under CO show that the reductive $[Fe^IFe^0]$ intermediates formed by the unsymmetrically disubstituted diiron complexes are not stable under argon. A considerable part of the $[Fe^IFe^0]$ intermediate is converted to a new complex by a quick chemical reaction which can be suppressed when the CV measurement is carried out under CO. The redox potentials of PR_3-disubstituted diiron dithiolate complexes can be adjusted in a range of ca. 200 mV.

Experimental Section

General Procedures: All reactions and operations related to organometallic complexes were carried out under dry oxygen-free dinitrogen using standard Schlenk techniques. Solvents were dried and distilled prior to use according to the standard methods. Commercially available chemicals, 1,3-propanedithol, $Fe(CO)_5$ and all tertiary phosphanes and phosphite compounds were reagent grade and used as received. Compounds $[(\mu\text{-pdt})Fe_2(CO)_5L]$ [L = PMe_3, **1**; PMe_2Ph, **2** and $P(OEt)_3$, **3**] and $[(\mu\text{-edt})Fe_2(CO)_5PMe_3]$ were prepared according to previously reported procedures.[15,25] Infrared spectra were recorded in CH_3CN solutions with a JASCO FT/IR 430 spectrophotometer. ^1H and $^{31}P\{^1H\}$ NMR spectra were recorded with a Varian INOVA 400 NMR spectrometer. Elemental analyses were performed with a Thermoquest-Flash EA 1112 elemental analyser and the mass spectra of the iron complexes were recorded with an HP1100 MSD instrument.

Synthesis of $[(\mu\text{-pdt})\{Fe(CO)_2PMe_3\}\{Fe(CO)_2L\}]$ [L = PMe_2Ph (4), PPh_3 (5), $P(OEt)_3$ (7)]: Complex **1** (0.43 g, 1.0 mmol) was treated with PMe_2Ph (0.14 g, 1.0 mmol) in toluene (40 mL) at reflux for 5 h. Complex **4** was obtained by column chromatography on neutral alumina with hexane and CH_2Cl_2 as gradient eluents. Yield: 0.11 g (40%). $C_{18}H_{26}Fe_2O_4P_2S_2$ (544.2): calcd. C 39.73, H 4.82; found C 39.77, H 4.87. ^1H NMR ($CDCl_3$): δ = 7.68, 7.42 (2 s, 5 H, Ph), 1.87 (s, 6 H, the CH_3 of PMe_2Ph), 1.67–1.56 (br. m, 6 H, $CH_2CH_2CH_2$), 1.45 (s, 9 H, PMe_3) ppm. $^{31}P\{^1H\}$ NMR ($CDCl_3$): δ = 30.99 (PMe_2Ph), 25.89 (PMe_3) ppm. IR (CH_3CN): $\tilde{\nu}$CO = 1981, 1943, 1907 cm^{-1}. APCI-MS: m/z = 544.8 $[M + H]^+$. Complex **5** was prepared according to a procedure similar to that of **4**, with PPh_3 (0.26 g, 1.0 mmol) as the ligand. Yield: 0.40 g (60%). $C_{28}H_{30}Fe_2O_4P_2S_2$ (668.3): calcd. C 50.32, H 4.52; found C 50.24, H 4.63. ^1H NMR ($CDCl_3$): δ = 7.75, 7.33 (2 s, 15 H, Ph), 1.47 (d, 9 H, PMe_3), 1.66–1.12 (br. m, 6 H, $CH_2CH_2CH_2$) ppm. $^{31}P\{^1H\}$ NMR ($CDCl_3$): δ = 62.81 (PPh_3), 25.66 (PMe_3) ppm. IR (CH_3CN): $\tilde{\nu}$CO = 1985, 1946, 1905 cm^{-1}. APCI-MS: m/z = 669.0 $[M + H]^+$. Complex **7** was prepared according to a similar procedure used for **4** but with $P(OEt)_3$ (0.17 g, 1.0 mmol) as the ligand. Yield: 0.36 g (62%). $C_{16}H_{30}Fe_2O_7P_2S_2$ (572.2): calcd. C 33.59, H 5.28; found C 33.71, H 5.18. ^1H NMR ($CDCl_3$): δ = 4.16 (s, 6 H, OCH_2), 1.46 (d, 9 H, PMe_3), 1.37 [s, 9 H, the CH_3 of $P(OEt)_3$], 1.61–1.21 (br. m, 6 H, $CH_2CH_2CH_2$) ppm. $^{31}P\{^1H\}$ NMR ($CDCl_3$): δ = 175.38 [$P(OEt)_3$], 27.10 (PMe_3) ppm. IR (CH_3CN): $\tilde{\nu}$ = CO = 1991, 1949, 1907 cm^{-1}. APCI-MS: m/z = 572.8 $[M + H]^+$.

Synthesis of $[(\mu\text{-pdt})\{Fe(CO)_2PMe_3\}\{Fe(CO)_2PCy_3\}]$ (6): Complex **6** can be obtained by using Me_3NO as a CO-removing reagent. A solution of complex **1** (0.43 g, 1.0 mmol) in CH_3CN (10 mL) was treated with $Me_3NO{\cdot}2H_2O$ (0.11 g, 1.0 mmol) at 50 °C for 30 min and PCy_3 (0.28 g, 1.0 mmol) was then added to the solution. The mixture was stirred for 1 h and the resultant solution concentrated to dryness under vacuum. The crude product was purified by flash column chromatography on neutral alumina with hexane/CH_2Cl_2 (1:1) as eluent. Yield: 0.15 g (22%). $C_{28}H_{48}Fe_2O_4P_2S_2$ (686.42): calcd. C 48.99, H 7.05; found C 48.93, H 6.94. ^1H NMR ($CDCl_3$): δ = 1.47 (s, 9 H, PMe_3), 2.12–1.29 (br. m, 39 H, $CH_2CH_2CH_2$ and PCy_3) ppm. $^{31}P\{^1H\}$ NMR ($CDCl_3$): δ = 68.54 (PCy_3), 23.49 (PMe_3) ppm. IR (CH_3CN): $\tilde{\nu}$CO = 1976, 1937, 1901 cm^{-1}. ESI-MS: m/z = 687.0 $[M + H]^+$.

Synthesis of $[(\mu\text{-pdt})\{Fe(CO)_2(PMe_2Ph)\}\{Fe(CO)_2L\}]$ [L = PPh_3 (8), $P(OEt)_3$ (9)]: Triphenylphosphane (0.26 g, 1.0 mmol) was added to a solution of complex $[(\mu\text{-pdt})Fe_2(CO)_5(PMe_2Ph)]$ (**2**) (0.50 g, 1.0 mmol) in toluene (40 mL). The solution was heated to reflux with stirring for 5 h, and the colour turned deep red. After the solution was concentrated by solvent evaporation under vac-

uum, the crude product was purified by column chromatography on neutral alumina with hexane/CH_2Cl_2 (2:1) as eluent. Product **8** was obtained by cooling the concentrated hexane/CH_2Cl_2 solution to –20 °C. Yield: 0.51 g (69%). $C_{33}H_{32}Fe_2O_4P_2S_2$ (730.4): calcd. C 54.27, H 4.42; found C 54.20, H 4.45. ^{1}H NMR ($CDCl_3$): δ = 7.72, 7.39 (2 br. s, 20 H, Ph), 1.79 (d, 6 H, the CH_3 of PMe_2Ph), 1.48–1.26 (br. m, 6 H, $CH_2CH_2CH_2$) ppm. $^{31}P\{^1H\}$ NMR ($CDCl_3$): δ = 62.95 (PPh_3), 32.98 (PMe_2Ph) ppm. IR (CH_3CN): $\tilde{\nu}$CO = 1982, 1946, 1913 cm^{-1}. APCI-MS: *m*/*z* = 731.0 [M + H]$^+$. Complex **9** was prepared according to a similar procedure used for **8** or by using complex **2** as a starting compound. The reaction of **2** (0.50 g, 1.0 mmol) with $P(OEt)_3$ (0.17 g, 1.0 mmol) was carried out in toluene. Yield: 0.40 g (64%). $C_{21}H_{32}Fe_2O_7P_2S_2$ (634.2): calcd. C 39.77, H 5.09; found C 39.77, H 5.15. ^{1}H NMR ($CDCl_3$): δ = 7.62, 7.38 (2 s, 5 H, Ph), 4.10 (s, 6 H, OCH_2), 1.77 (s, 6 H, the CH_3 of PMe_2Ph), 1.32 [s, 9 H, the CH_3 of $P(OEt)_3$], 1.52–1.20 (br. m, 6 H, $CH_2CH_2CH_2$) ppm. $^{31}P\{^1H\}$ NMR ($CDCl_3$): δ = 175.15 [$P(OEt)_3$], 34.38 (PMe_2Ph) ppm. IR (CH_3CN): $\tilde{\nu}$CO = 1991, 1952, 1922 cm^{-1}. ESI-MS: *m*/*z* = 634.8 [M + H]$^+$.

Synthesis of [(μ-pdt){Fe(CO)$_2$P(OEt)$_3$}{Fe(CO)$_2$L}] [L = PPh$_3$ (10), PCy$_3$ (11)]: A solution of [(μ-pdt)$Fe_2(CO)_5P(OEt)_3$] (**3**) (0.52 g, 1.0 mmol) in CH_3CN (15 mL) was treated with $Me_3NO{\cdot}2H_2O$ (0.11 g, 1.0 mmol) at room temperature. The red solution was stirred for 15 min and turned dark red. Triphenylphosphane (0.26 g, 1.0 mmol) was added to the mixture in one portion with stirring. The reaction mixture was stirred for 20 min, and the resultant solution was concentrated to dryness under vacuum. The crude product was purified by flash column chromatography on neutral alumina with hexane/CH_2Cl_2 (1:1) as eluent. Product **10** was obtained by cooling the concentrated hexane/CH_2Cl_2 solution to –20 °C. Yield: 0.54 g (72%). $C_{31}H_{36}Fe_2O_7P_2S_2$ (758.4): calcd. C 49.10, H 4.78; found C 49.12, H 4.89. ^{1}H NMR ($CDCl_3$): δ = 7.74, 7.41 (2 s, 15 H, Ph), 4.15 (s, 6 H, OCH_2), 1.55 (br. s, 6 H, $CH_2CH_2CH_2$), 1.35 [s, 9 H, CH_3 of $P(OEt)_3$] ppm. $^{31}P\{^1H\}$ NMR ($CDCl_3$): δ = 175.00 [$P(OEt)_3$], 64.19 (PPh_3) ppm. IR (CH_3CN): $\tilde{\nu}$CO = 1997, 1955, 1934 cm^{-1}. ESI-MS: *m*/*z* = 759.1 [M + H]$^+$. Complex **3** (0.52 g, 1.0 mmol) was treated with PCy_3 (0.14 g, 1.0 mmol) in toluene (40 mL) at reflux for 6 h. Complex **11** was obtained by column chromatography on neutral alumina with hexane and CH_2Cl_2 as gradient eluents. Yield: 0.51 g (65%). $C_{31}H_{54}Fe_2O_7P_2S_2$ (776.5): calcd. C 47.95, H 7.01; found C 47.68, H 6.94. ^{1}H NMR ($CDCl_3$): δ = 4.18 (s, 6 H, OCH_2), 1.38 [s, 9 H, CH_3 of $P(OEt)_3$], 2.12–1.29 (br. m, 39 H, $CH_2CH_2CH_2$ and PCy_3) ppm. $^{31}P\{^1H\}$ NMR ($CDCl_3$): δ = 174.77 [$P(OEt)_3$], 69.97 (PCy_3) ppm. IR (CH_3CN): $\tilde{\nu}$CO = 1993, 1943, 1933 cm^{-1}. ESI-MS: *m*/*z* = 777.2 [M + H]$^+$.

Synthesis of [(μ-edt){Fe(CO)$_2$PMe$_3$}{Fe(CO)$_2$PPh$_3$}] (12): Complex [(μ-edt){$Fe(CO)_2PMe_3$}{$Fe(CO)_3$}] (0.42 g, 1.0 mmol) was treated with PPh_3 (0.26 g, 1.0 mmol) in toluene (40 mL) at reflux for 5 h. The workup of complex **12** was similar to that for **5**. Yield: 0.42 g (64%). $C_{27}H_{28}Fe_2O_4P_2S_2$ (654.3): calcd. C 49.56, H 4.31; found C 49.78, H 4.54. ^{1}H NMR (CD_3COCD_3): δ = 7.65 (m, 9 H, Ph), 7.50 (s, 6 H, Ph), 1.81 (d, 2 H, CH_2), 1.53 (d, 9 H, PMe_3), 1.06 (d, 2 H, CH_2) ppm. $^{31}P\{^1H\}$ NMR ($CDCl_3$): δ = 60.31 (PPh_3), 22.68 (PMe_3) ppm. IR (CH_3CN): $\tilde{\nu}$CO = 1982, 1945, 1907 cm^{-1}. APCI-MS: *m*/*z* = 654.9 [M + H]$^+$.

X-ray Structure Determination of Complexes 4–6, 8–10 and 12: The single-crystal X-ray diffraction data were collected with an AFE5R Rigaku diffractometer for **4**, **8** and **9** and a Siemens SMART CCD diffractometer for **5**, **6**, **10** and **12**, with graphite-monochromated Mo-K_α radiation (λ = 0.071073 Å) at 293 K using the ω-2θ scan mode. Data processing was accomplished with the SAINT processing program.[29] Intensity data for **4**–**6** and **8**–**10** were corrected for absorption using the SADABS program.[30] All structures were solved by direct methods and refined on F^2 against full-matrix least-squares methods by using the SHELXTL97 program package.[31] All non-hydrogen atoms were refined anisotropically. Hydrogen atoms were located by geometrical calculation. Details of crystal data, data collections and structure refinements are summarised in Tables 4 and 5. CCDC-627499 (**4**), -627500 (**5**), -627501 (**6**), -627502 (**8**), -627503 (**9**), -627504 (**10**) and -630623 (**12**) contain the supplementary crystallographic data for this paper. These data can be obtained free of charge from The Cambridge Crystallographic Data Centre via www.ccdc.cam.ac.uk/data_request/cif.

Table 4. Crystallographic data and processing parameters for complexes **4**–**6**.

Complex	**4**	**5**	**6**
Empirical formula	$C_{18}H_{26}Fe_2O_4P_2S_2$	$C_{28}H_{30}Fe_2O_4P_2S_2$	$C_{28}H_{48}Fe_2O_4P_2S_2$
Formula mass	544.15	668.28	686.42
Crystal system	monoclinic	monoclinic	monoclinic
Space group	$P2_1/n$	$P2_1/n$	$P2_1/c$
a [Å]	14.802(3)	8.431(2)	11.992(1)
b [Å]	10.337(2)	22.350(5)	12.077(1)
c [Å]	16.090(3)	16.403(4)	22.658(3)
α [°]	90	90	90
β [°]	105.53(3)	93.598(3)	98.146(1)
γ [°]	90	90	90
V [Å^3]	2372.0(8)	3085.0(12)	3248.3(6)
Z	4	4	4
$D_{calcd.}$ [g cm^{-3}]	1.524	1.439	1.404
Crystal size [mm]	0.15 × 0.28 × 0.30	0.08 × 0.16 × 0.22	0.20 × 0.26 × 0.32
$\theta_{min/max}$ [°]	3.29–27.44	2.21–27.00	1.92–27.00
Reflections collected	5395	6727	7064
Unique data, R_{int}	4694, 0.0242	5325, 0.0262	5223, 0.0403
Parameters	253	343	343
GOF on F^2	1.074	1.067	1.009
R_1 [$I > 2\sigma(I)$]	0.0278	0.0322	0.0369
wR_2 [$I > 2\sigma(I)$]	0.0676	0.0767	0.0793
Residual electron density [e Å^{-3}]	1.067,–0.501	0.382, –0.259	0.325, –0.301

Table 5. Crystallographic data and processing parameters for complexes **8**–**10** and **12**.

Complex	**8**·0.5C_6H_{14}	**9**	**10**	**12**
Empirical formula	$C_{33}H_{32}Fe_2O_4P_2S_2$·0.5$C_6H_{14}$	$C_{21}H_{32}Fe_2O_7P_2S_2$	$C_{31}H_{36}Fe_2O_7P_2S_2$	$C_{27}H_{28}Fe_2O_4P_2S_2$
Formula mass	773.43	634.23	758.36	654.25
Crystal system	triclinic	triclinic	orthorhombic	orthorhombic
Space group	$P\bar{1}$	$P\bar{1}$	*Pbca*	$P2_12_12_1$
a [Å]	10.780(5)	8.600(2)	20.154(3)	12.2677(2)
b [Å]	12.459(5)	11.586(2)	15.815(2)	15.1411(3)
c [Å]	14.972(7)	15.036(3)	21.852(3)	16.1701(3)
α [°]	79.304(14)	96.25(3)	90	90
β [°]	84.660(14)	92.93(3)	90	90
γ [°]	69.358(10)	105.13(3)	90	90
V [Å ^{3}]	1848.2(15)	1432.7(5)	6965.2(18)	3003.54(10)
Z	2	2	8	4
$D_{calcd.}$ [g cm^{-3}]	1.390	1.470	1.446	1.447
Crystal size [mm]	0.12 × 0.13 × 0.25	0.10 × 0.24 × 0.30	0.12 × 0.28 × 0.30	0.30 × 0.40 × 0.52
$\theta_{min/max}$ [°]	2.06–28.28	2.99–27.45	1.86–26.00	1.84–30.00
Reflections collected	8963	6369	6852	8482
Unique data, R_{int}	7411, 0.0174	4515, 0.0381	5741, 0.0298	7146, 0.0322
Parameters	425	307	398	353
GOF on F^2	1.055	1.058	1.057	1.006
R_1 [$I > 2\sigma(I)$]	0.0464	0.0501	0.0315	0.0304
wR_2 [$I > 2\sigma(I)$]	0.1222	0.1378	0.0810	0.0657
Residual electron density [e Å^{-3}]	0.940, –0.539	0.857, –0.695	0.732, –0.551	0.241, –0.299

Electrochemical Studies of Complexes 4–11: Cyclic voltammograms were obtained in a three-electrode cell under argon using a BAS 100B electrochemical workstation. The working electrode was a glassy carbon disk (0.071 cm^2) polished with 3 and 1 μm diamond pastes and sonicated for 10 min prior to use. The reference electrode was a non-aqueous Ag/Ag$^+$ (0.01 M $AgNO_3$ in CH_3CN) electrode and the counter electrode was a platinum wire. A solution of 0.05 M nBu$_4$NPF$_6$ (Fluka, electrochemical grade) in CH_3CN was used as the supporting electrolyte for complexes **4**, **5** and **7**–**10**. A mixed solution of 0.05 M nBu$_4$NPF$_6$ (Fluka, electrochemical grade) in toluene and acetonitrile (1:3, v/v) was used as supporting electrolyte for complexes **6** and **11** due to its poor solubility in pure CH_3CN. Acetonitrile (Aldrich, spectroscopic grade) used for electrochemical measurements was freshly distilled from CaH_2 under N_2.

Supporting Information (see footnote on the first page of this article): Cyclic voltammograms of complexes **4**, **6**–**8**, **10** and **11** under argon and CO, as well as the multiple scans for complex **5** at a scan rate of 4.0 V s^{-1} are included.

Acknowledgments

We are grateful to the Chinese National Natural Science Foundation (Grant nos. 20471013 and 20633020), the Swedish Energy Agency, the Swedish Research Council and the K & A Wallenberg Foundation for financial support of this work.

[1] J. W. Peters, W. N. Lanzilotta, B. J. Lemon, L. C. Seefeldt, *Science* **1998**, *282*, 1853–1858.
[2] Y. Nicolet, C. Piras, P. Legrand, C. E. Hatchikian, J. C. Fontecilla-Camps, *Structure* **1999**, *7*, 13–23.
[3] E. J. Lyon, I. P. Georgakaki, J. H. Reibenspies, M. Y. Darensbourg, *Angew. Chem. Int. Ed.* **1999**, *38*, 3178–3180.
[4] M. Schmidt, S. M. Contakes, T. B. Rauchfuss, *J. Am. Chem. Soc.* **1999**, *121*, 9736–9737.
[5] A. L. Cloirec, S. P. Best, S. Borg, S. C. Davies, D. J. Evans, D. L. Hughes, C. J. Pickett, *Chem. Commun.* **1999**, 2285–2286.
[6] E. J. Lyon, I. P. Georgakaki, J. H. Reibenspies, M. Y. Darensbourg, *J. Am. Chem. Soc.* **2001**, *123*, 3268–3278.
[7] L. Song, J. Ge, X. Zhang, Y. Liu, Q. Hu, *Eur. J. Inorg. Chem.* **2006**, 3204–3210.
[8] F. Gloaguen, J. D. Lawrence, T. B. Rauchfuss, *J. Am. Chem. Soc.* **2001**, *123*, 9476–9477.
[9] F. Gloaguen, J. D. Lawrence, M. Schmidt, S. R. Wilson, T. B. Rauchfuss, *J. Am. Chem. Soc.* **2001**, *123*, 12518–12527.
[10] F. Gloaguen, J. D. Lawrence, T. B. Rauchfuss, M. Bénard, M. Rohmer, *Inorg. Chem.* **2002**, *41*, 6573–6582.
[11] X. Zhao, I. P. Georgakaki, M. L. Miller, J. C. Yarbrough, M. Y. Darensbourg, *J. Am. Chem. Soc.* **2001**, *123*, 9710–9711.
[12] M. M. Hasan, M. B. Hursthouse, S. E. Kabir, K. M. A. Malik, *Polyhedron* **2001**, *20*, 97–101.
[13] X. Zhao, I. P. Georgakaki, M. L. Miller, R. Mejia-Rodriguez, C. Chiang, M. Y. Darensbourg, *Inorg. Chem.* **2002**, *41*, 3917–3928.
[14] R. Mejia-Rodroguez, D. Chong, J. H. Reibenspies, M. P. Soriaga, M. Y. Darensbourg, *J. Am. Chem. Soc.* **2004**, *126*, 12004–12014.
[15] P. Li, M. Wang, C. He, G. Li, X. Liu, C. Chen, B. Åkermark, L. Sun, *Eur. J. Inorg. Chem.* **2005**, 2506–2513.
[16] J. Hou, X. Peng, Z. Zhou, S. Sun, X. Zhao, S. Gao, *J. Organomet. Chem.* **2006**, *691*, 4633–4640.
[17] Y. Na, M. Wang, K. Jin, R. Zhang, L. Sun, *J. Organomet. Chem.* **2006**, *691*, 5045–5051.
[18] J. D. Lawrence, T. B. Rauchfuss, S. R. Wilson, *Inorg. Chem.* **2002**, *41*, 6193–6195.
[19] J. L. Nehring, D. M. Heinekey, *Inorg. Chem.* **2003**, *42*, 4288–4292.
[20] J. Capon, S. E. Hassnaoui, F. Gloaguen, P. Schollhammer, J. Talarmin, *Organometallics* **2005**, *24*, 2020–2022.
[21] J. W. Tye, J. Lee, H. Wang, R. Mejia-Rodriguez, J. H. Reibenspies, M. B. Hall, M. Y. Darensbourg, *Inorg. Chem.* **2005**, *44*, 5550–5552.
[22] J. I. Vlugt, T. B. Rauchfuss, C. M. Whaley, S. R. Wilson, *J. Am. Chem. Soc.* **2005**, *127*, 16012–16013.
[23] W. Dong, M. Wang, X. Liu, K. Jin, G. Li, F. Wang, L. Sun, *Chem. Commun.* **2006**, 305–307.
[24] L. Schwartz, G. Eilers, L. Eriksson, A. Gogoll, R. Lomoth, S. Ott, *Chem. Commun.* **2006**, 520–522.
[25] L. E. Bogan, D. A. Lesch, T. B. Rauchfuss, *J. Organomet. Chem.* **1983**, *250*, 429–438.
[26] M. Y. Darensbourg, E. J. Lyon, X. Zhao, I. P. Georgakaki, *Proc. Natl. Acad. Sci.* **2003**, *100*, 3683–3688.

[27] J. Ekström, M. Abrahamsson, C. Olson, J. Bergquist, F. B. Kaynak, L. Eriksson, L. Sun, H. Becker, B. Åkermark, L. Hammarström, S. Ott, *Dalton Trans.* **2006**, 4599–4606.
[28] D. Chong, I. P. Georgakaki, R. Mejia-Rodriguez, J. Sanabria-Chinchilla, M. P. Soriaga, M. Y. Darensbourg, *Dalton Trans.* **2003**, 4158–4163.
[29] *Software packages SMART and SAINT*, Siemens Energy & Automation Inc., Madison, Wisconsin, **1996**.
[30] G. M. Sheldrick, *SADABS, Absorption Correction Program*, University of Göttingen, Germany, **1996**.
[31] G. M. Sheldrick, *SHELXTL97, Program for the Refinement of Crystal Structure*, University of Göttingen, Germany, **1997**.
Received: December 13, 2006
Published Online: June 18, 2007

